DSTO

Evaluation of Underwater Explosive Performance of PBXW-115 (AUST)

G. Bocksteiner

DTIC

APPROVED FOR PUBLIC RELEASE

DEPARTMENT ◆ OF DEFENCE
DEFENCE SCIENCE AND TECHNOLOGY ORGANISATION

Evaluation of Underwater Explosive Performance of PBXW-115 (AUST)

G. Bocksteiner

Weapons Systems Division
Aeronautical and Maritime Research Laboratory

DSTO-TR-0297

ABSTRACT

An investigation has been carried out on the underwater explosive performance properties of Australian-made PBXW-115, a polymer bonded explosive (PBX) made from AP / bimodal RDX / Al in a plasticised polyurethane binder. The following underwater performance parameters of 25 kg PBX-115 charges, detonated by a central core of pentolite, have been measured: peak pressure, time constant, shock impulse, energy flux density, shock wave energy, relative bubble energy and the similitude constants have been evaluated. The shock wave energy (E_{SW}) of PBXW-115 (Aust) is 1.85 and its bubble energy (E_{RB}) is 2.25, relative to the accepted standard, pentolite (values 1.00), for each parameter); these values compare to those from Composition H-6 (E_{SW} 1.18, E_{RB} 1.54) probably the most commonly used and best known underwater explosive amongst the current inventories of the navies of the world. These data suggest that PBXW-115 should be a superior fill for use in underwater blast weapons.

RELEASE LIMITATION

Approved for Public Release

DEPARTMENT OF DEFENCE

DEFENCE SCIENCE AND TECHNOLOGY ORGANISATION

Published by

DSTO Aeronautical and Maritime Research Laboratory
PO Box 4331
Melbourne Victoria 3001

Telephone: (03) 9626 8111
Fax: (03) 9626 8999

AR No. AR-009-488
February 1996

Approved for Public Release

Evaluation of Underwater Explosive Performance of PBXW-115 (AUST)

Executive Summary

This is a report on assessment of the underwater explosive performance of a polymer bonded explosive, PBXW-115 (Aust.), an explosive fill developed at AMRL. This polymer bonded explosive was designed to meet insensitive munitions (IM) criteria. However meeting the explosives IM criteria is quite often achieved at the expense of explosive performance, a trade-off normally considered unacceptable. This work was undertaken to assess whether the explosive performance of PBXW-115(Aust.) was satisfactory in comparison with conventional underwater explosives.

The Australian formulated PBXW-115 underwater explosive was found to have shock wave energy and relative bubble energy output greater than that of currently conventional underwater explosives H-6 and Torpex. It was also found to be comparable with , if not greater than, the warhead fills used by the RAN in its current weapons inventory.

The methodology used in assessing underwater performance of the PBXW-115 explosive at AMRL provides a more realistic assessment of the underwater performance potential of this material than previously used approaches. The shock wave energy and bubble energy of PBXW-115 (Aust) are respectively 1.85 and 2.25 times that of the accepted standard pentolite.

These explosive performance parameters suggest that PBXW-115 should be a superior fill for use in underwater blast weapons.

The Director of Armament Engineering - Navy is proposing this PBX as the warhead fill for the mine demolition charge as part of the Mine Hunter Coastal Defence System inventory.

Authors

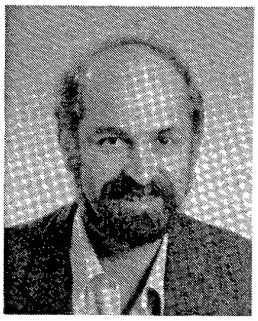

G. Bocksteiner
Weapons Systems Division

Gunter Bocksteiner graduated from Footscray Institute of Technology in Applied Chemistry and joined AMRL in 1968. He has worked widely within AMRL, initially on the mechanistic chemistry of chemiluminescent materials, then biologically active surface coatings and the effects of the marine environment on defence materiel. In 1980 he commenced work on determination of explosives hazard, and since 1987 has been working on polymer bonded explosives formulations.

Contents

1. Introduction

PBXW-115 is a polymer bonded explosive (PBX) which was developed at Naval Surface Warfare Center, White Oak, Silver Spring, MD, USA in the late 70s / early 80s, for potential use as an insensitive explosive fill for underwater applications [1].
Since that time, PBXW-115 has been fully qualified, accepted as a possible insensitive munitions (IM) warhead fill by the US Navy and renamed PBXN-111 [2]. The use of PBXN-111 as the mine neutralisation charge designated Mk 98 MNC is currently under consideration by the US Navy [3].

Indications from recently received information [4] are that three different formulations closely related to PBXN-111 have been either developed or introduced into service in Europe since 1991. Great Britain has developed one formulation for underwater applications, ROWANEX 1301, the first part of the name being an acronym for Royal Ordnance Waltham Abbey Naval Explosive [4]. There is also a German equivalent, KS 57, which has been developed by Messerschmitt-Bölkow-Blohm (MBB) GmbH, made from bimodal RDX (24%) / Al (24%) / AP (40%) / plasticised HTPB binder (12%) [4-6], and two SNPE (France) PBXN-111 - styled fills, called B2211B and B2211D. These last two formulations have been incorporated in the warheads of the current versions of the UK-based Marconi mine, Stonefish [4, 7].

The Australian version of PBXW-115, designated as PBXW-115 (Aust.), has recently been developed [8] and reports related to the binder chemistry and explosive properties have either been published or are in the process of publication [8-12].

PBXW-115 (Aust.) has also been type-qualified by the Australian Ordnance Council [13] and is currently under consideration for use as a potential main charge fill in mine neutralisation charges.

PBXW-115 (Aust.) appears to have some properties which differ from those of its US counterpart (larger critical diameter, lower limiting velocity of detonation, lower sensitivity to shock, etc.) [1, 11, 14].

In this report, the underwater performance of 25 kg cylinders of PBXW-115 (Aust.) has been investigated, with respect to its underwater blast and relative bubble energy properties. Comments have also been made on scaling factors, charge design and charge configuration in an attempt to reconcile the results obtained here compared to those reported for PBXW-115 of US origin in a different configuration [15].

2. Underwater Explosions

A comprehensive description of the sequence of events that take place in an underwater explosion and the scientific principles needed to analyse such events can be found in the account by Cole [16]; a less detailed, but nevertheless useful, summary is provided in the *Encyclopedia of Explosives and Related Items* [17].

An attempt is made in this report to briefly describe and define relevant events using in part the observations for the underwater explosive performance experiments conducted at AMRL's underwater explosives test facility.

2.1 Basic Concepts

When an explosive charge is detonated in deep water, the total energy liberated from such an event is partitioned into radiated shock wave energy and bubble energy, the degree of partitioning being determined by the explosive type and the distance from the explosive event [16-19].

In addition, it has been observed that the more intense the shock wave, the greater the adiabatic heating of surrounding water, and this results in a corresponding reduction in the available energy contributed to the pulsating bubble following the shock wave.

Hicks has reported on the factors which must be addressed to optimise underwater explosive performance [18] and has also described quantitatively where the energy associated with the explosion is distributed (Figure 2). In his model, some of the shock wave energy is eventually transformed into bubble energy and this occurs some 20 charge radii from the explosion source; such a transformation accounts for an apparent 110% total energy output in Figure 1.

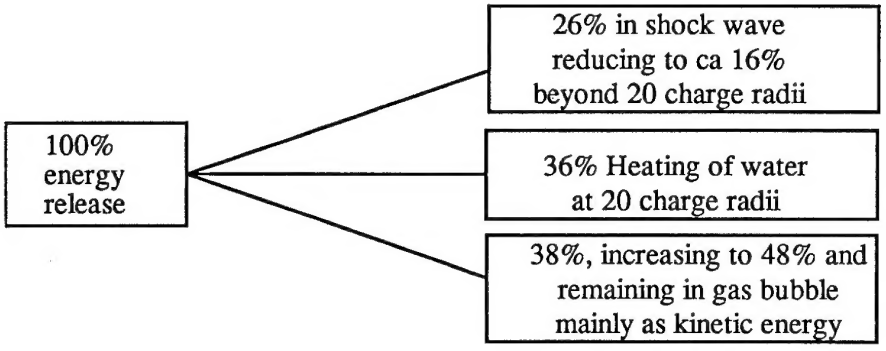

Figure 1. Energy distribution from an underwater explosion.

It is unwise to choose explosives with high detonation pressures for underwater applications if the efficiency of the bubble energy damage potential is to be maximised.

2.2 Underwater Explosive Test Sites: General Considerations

The ideal location for carrying out explosive performance testing is in a deep ocean so that effective performance comparisons can be made. Ideally, boundary effects such as reflections of shock waves from the bottom, surface and enclosing walls of the water

mass are then absent. However deep open ocean explosive performance testing is very expensive and is usually impractical for work such as that described herein.

For this reason, explosive performance measurements are made in confined bodies of water such as deep rivers, coastal waters subjected to large tidal depth fluctuations or deep water-filled quarry sites. In all of these cases, corrections must then be made to any experimental measurements for those boundary effects which invariably interfere with the prime pressure pulse generated by the initial detonation.

2.3 AMRL Underwater Explosive Test Facility

The underwater explosives test facility used by AMRL is located at Epping, Melbourne, in a flooded quarry where the average depth of water at "point zero", the location of the test charge on firing, is 16 metres. Test charges are placed below the surface of the water so as to minimise effects of surface cut-off and are so located that the quarry wall shock wave reflections give minimum interference to the measured pressure / time profiles. Salinity, pH and water temperature inclines are recorded regularly for calibration purposes.

The maximum permissible mass of explosive charge that can be fired at this quarry is 25 kg.

2.4 Instrumentation: Gauges and Rigging

The underwater pressure transducers (gauges) used in this investigation were PCB 138 A05 and A10 type gauges containing a tourmaline crystal sensing element. The outputs from these gauges were recorded directly onto an 80 kHz analogue bandwidth tape recorder.

An array of ten tourmaline underwater pressure gauges was laid out at various radial distances from the centre of the charge as shown in Figure 2. Two steel cables were strung across the quarry and the charge was suspended beneath a flying fox which was attached to one of these cables. Nine of the gauges were hung from the second cable at various distances from the charge, and the tenth gauge (the one closest to the charge) was hung from the first cable. All gauges and each of the PBXW-115 charges were located 8 m from the surface.

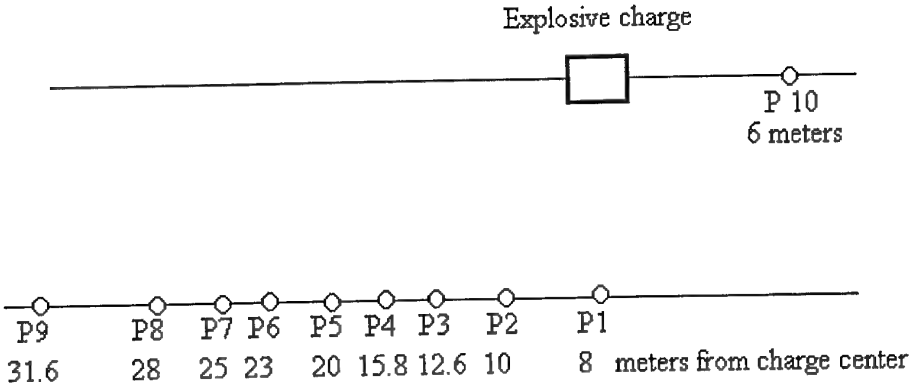

Figure 2: Radial pressure gauge lay out in relation to test charge

The sensitivities of the gauges were selected in accordance with their proximity of the test charge. All gauges were calibrated hydrostatically and dynamically with the output from 500 g standard pentolite shots.

Spacing between gauges was selected to cover the pressure range between 3 - 30 MPa over a maximum distance of 31.6 m.

Three infield and two midfield gauges (P10, 1, 2, 3 and 4) were located in the high pressure region of the explosive event (30 - 10 MPa) so that useful data in the damage range of interest could be observed. The position of the first high pressure gauge P10 was located at 6 m from the charge, a distance which is just outside the range of the estimated maximum bubble radius, 5.2 metres, that can be anticipated from a 25 kg PBXW-115 charge fired at 8 m depth (refer Section 5.4). The disruptive effect of the expanding bubble on this gauge is thereby avoided and at the same time gauge mortality rate is minimised. Two midfield and the remaining far field gauges (P5, 6, 7, 8 and 9) were located in the medium to low pressure region of the event.

2.5 Evaluation of Underwater Explosive Performance

An evaluation of underwater explosive performance is made by comparing the following performance parameters,
peak pressures (P_m),
time constants (θ),
impulse (I),
energy flux (E)
relative bubble energy (E_{RB})
with those of a standard explosive such as trinitrotoluene (TNT) or pentolite.

The shock wave energy (E_{SW}) is primarily a function of P_m, θ, I and E and is compared either on an equal mass or equal volume basis with the corresponding value for standard TNT or pentolite. In this work equal mass comparisons were used.

The bubble energy is primarily a function of both the bubble period and the mass of explosive used; again, output is compared to that from standard TNT or pentolite; the comparison factor is normally referred to as the relative bubble energy.

The term "shock factor", is sometimes reported; its value is intended to assess the potential of an explosive formulation to inflict structural damage to a target. It is not the purpose of this report to address the damage potential these parameters have on specific structural targets. Therefore only a brief introduction to shock factor terminology is given in Section 4.9.

3. PBXW-115 Charges

3.1 Charge Size

Two right cylinder shaped PBXW-115 explosive charges were assessed for their underwater performance (Events 1 and 2). The charges used in Event 1 and 2 had a density of 1.79 Mgm^{-3}, masses of 24.8 and 24.9 kg PBXW-115 respectively.

3.2 Formulation

Extensive details on PBXW-115 formulation, chemistry of the binder [8], methods of manufacture, recommendations for charge size selection and design have been reported elsewhere [9]. The formulation of PBXW-115 is given in Table 1.

3.3 Initiating System

A spherical centrally located booster consisting of 0.5 kg of 50/50 pentolite and a N° 8 ICI detonator was used to initiate the main charge. The density of the pentolite boosters was 1.65 Mgm^{-3}.

Table 1: Formulation of PBXW-115 and its US counterpart, PBXN-111.

COMPONENT	MASS (%)	BINDER (%)
Ammonium perchlorate (200 μm)	43	
Aluminium X81 (20 μm)	25	
RDX Type I, Class I (200 μm)	12	
RDX Type II, Class 5 (20 μm)	8	
Hydroxyl terminated poly butadiene	5.7	47.5
Isodecylpelargonate	5.7	47.5
Isophorone diisocyanate	0.54	4.56
4,4'-methylene-bis(2,6-di-t-butylphenol)	0.05	0.417
Dibutyltin dilaurate	0.004	0.033

3.4 Configuration of Charge Assembly

The PBXW-115 main charge consisted of six cylindrical discs that were cast into suitably prepared cylindrical containers [9]. Where necessary the face of each disc was machined to ensure that no gaps existed between the interfaces of the final assembly. Two circular plywood endplates were used to clamp the discs in place and maintain rigidity during handling and placement of the charge at the point of firing.

A cross sectional view of the charge assembly with booster configuration is given in Figure 3a and an assembled perspective is shown in Figure 3b.

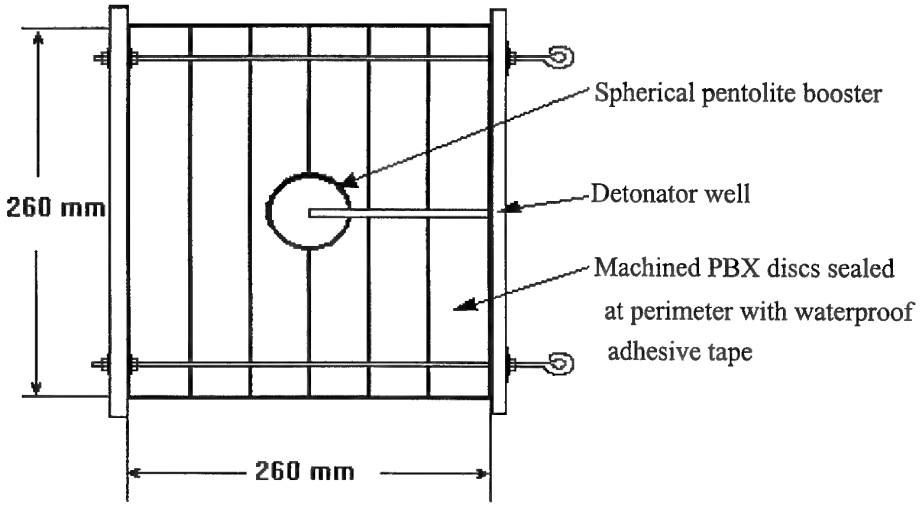

Figure 3a: 25 kg PBXW-115 charge assembly rig

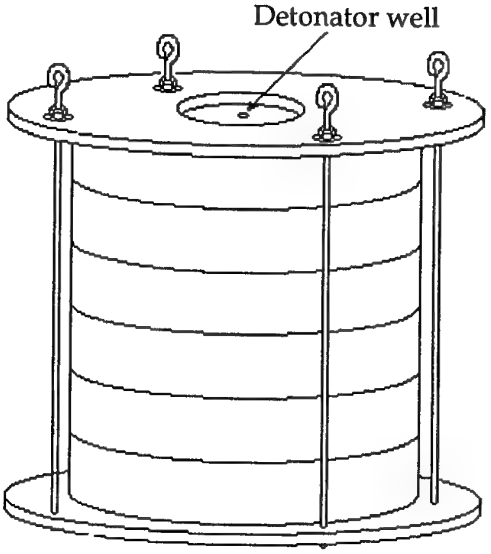

Figure 3b: Perspective view of charge assembly

4. Parameters for Underwater Explosive Performance Measurements

4.1 The Shock Wave of an Underwater Detonation

As stated in Section 2, there are two main events following the detonation of an underwater explosion. The first can be described in terms of the generation and transmission of the initial shock wave. This shock wave is transmitted on the millisecond time scale. The second event, the pulsed expansion and contraction of the bubble of gaseous products of detonation, occurs on a much larger time scale, the hundreds of milliseconds range.

To measure the shock wave at the AMRL test site, pressure gauge measurements were recorded every 0.2 μ seconds. A profile of a typical shock wave pressure time curve at increasing distances from the explosive charge demonstrating the scalar relationship of peak pressure (P_m), here nominally 28 MPa, and its rapid depletion at nominal distances from 6 to 24 metres, is shown in Figure 4.

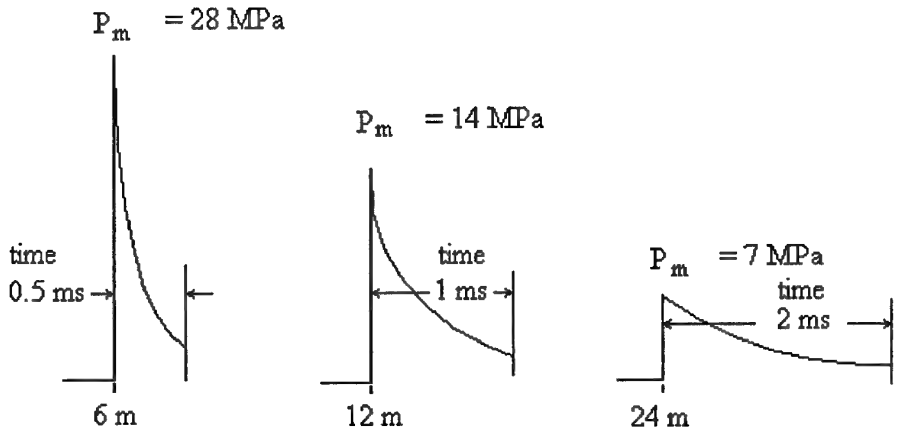

Figure 4: An idealised model of the shock wave pressure- time curves from an explosive charge at distances of 6 m, 12 m and 24 m.

4.2 Peak Pressure and Time Constant Relationship

It is generally accepted and has been empirically established that the mathematical approximation for the resulting shock wave pressure / time curve decays exponentially according to Equation 1 [16, 19].

$$P(t) = P_m e^{-t/\theta} \qquad (1)$$

where P(t) is the recorded pressure as a function of time t, P_m is the initial peak pressure and θ is the time constant for the initial decay process.

4.3 Time Constant, θ

The time constant, θ, as defined in Equation 1 can be regarded as the time taken for peak pressure (P_m) to decay to a value equal to P_m /e.

A graphical interpretation of the mathematical relationship as defined by the exponential in Equation 1 (solid line) is given in Figure 5 where t_1 denotes the time of arrival of the shock wave and t_2, the time elapsed after one time constant of exponential pressure decay. After this time, θ, the actual P(t) - time plot has been found to begin to deviate from Equation 1; while auxiliary functions can be introduced to fit the latter portions of the plot they seldom shed any additional light on the processes affecting the performance of the explosive.

The dashed line in Figure 5 represents the region where the decay in shock wave pressure departs from the relationship as defined by Equation 1 and follows an observed course of slower rate in exponential decay.

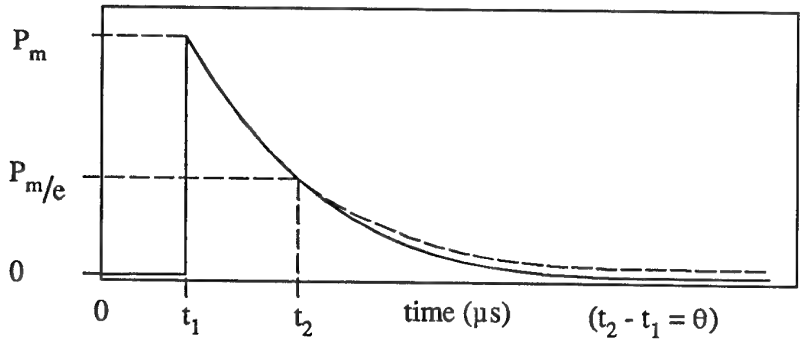

Figure 5: Shock wave pressure time plot without boundary influences outlining the course of natural (solid line) and observed (dashed line) exponential decay.

4.3.1 Similitude Equations

By application of "The Principle of Similarity" [16,19], it has been found that underwater shock wave parameters, P_m, θ, I or E, follow a dependency of the form

$$\text{Parameter} = k\left(\frac{W^{1/3}}{R}\right)^{\alpha} \qquad (2)$$

The parameters, P_m, θ, I and E are experimentally determined while the constants, k and α, the similitude constants, are characteristic of the explosive under tests.

The logarithmic form of Equation 2 is

$$\ln(\text{Parameter}) = \ln k + \alpha/3 \ln W - \alpha \ln R \qquad (3)$$

suggesting that a logarithmic plot of any of the parameters P_m, θ, I and E against ln R will produce a straight line with a gradient equal to $-\alpha$.

4.3.2 Time Constant and Distance from Charge Relationship

Time constants are derived from pressure versus time profiles as explained above.

Pressure versus time profiles for each event were obtained from each of the ten pressure gauges set at nominal distances, R_n, from the PBX charge. Corrected gauge distances from the charge centre, R_c, for each event were obtained by using a time-of-arrival calibration method (Section 5.6) and are listed in Table 2.

Table 2: Nominal and Corrected Distances in Metres from Charges.

Gauge N°	P10	P1	P2	P3	P4	P5	P6	P7	P8	P9
R_n m	6	8	10	12.6	15.8	20	23	25	28	31.6
R_c m Event 1	6.5	8.1	9.8	12.2	15.3	19.4	22.5	24.5	27.4	31.1
R_c m Event 2	6.5	8.1	9.7	12.2	15.3	19.4	22.5	24.4	27.3	31.1
R_c mean Event 1 & 2	6.5	8.1	9.8	12.2	15.3	19.4	22.5	24.5	27.4	31.1

Because there were only small differences observed in the corrected gauge distances, R_c, for the two events, mean values of R_c were used in all calculations.

In Figure 6, plots of ln θ versus ln R (where R is the distance of the charge from the pressure gauge) have been made for data obtained from cast TNT and pentolite. The θ values for TNT and pentolite were obtained from an extensive data base compiled from experiments conducted presumably under ideal conditions [19].

Plots of ln θ versus ln R drawn from data on PBXW-115 (Aust.) obtained in this program of work are also shown in Figure 6.

Table 3: Time constant readings recorded at nominal and corrected distances from charge centre for 25 kg of TNT, Pentolite and PBXW-115 (Event 1, and 2).

Function			Time constant θ				
			PBXW-115			TNT	Pentolite
Gauge	Distance m		Event 1	Event 2	Average		
N°	R_n	R_c	μs	μs	μs	μs	μs
P10	6.0	6.5	467	434	451	284	284
P1	8.0	8.1	379	367	373	303	303
P2	10.0	9.8	422	449	434	320	320
P3	12.6	12.2	447	444	446	336	336
P4	15.8	15.3	480	497	489	354	354
P5	20.0	19.4	480	495	495	375	375
P6	23.0	22.5	500	505	494	386	386
P7	25.0	24.5	483	-	483	395	395
P8	28.0	27.4	-	-	-	405	405
P9	31.6	31.1	502	529	516	415	415

The PBXW-115 data reported in this work is based on single sets of gauge readings for each event; as the measurements were conducted at a non ideal quarry site, there is a considerable degree of point scattering present.

The closest gauge (P10) had twice the maximum pressure threshold of the mid-field and far-field gauges and appears to have recorded a higher-than-expected response for θ as a result of better signal resolving power. The second in-field gauge (P1), which experienced a peak pressure close to its maximum pressure threshold recorded a lower-than-expected response for θ. This low response may be attributed to this gauge being deployed at the limit of its operating range. The mid field gauges (P3, P4, P5 and P6) appeared to respond as anticipated. The far-field gauges (P7, P8 and

P9) show evidence of interference from boundary reflections. The value of θ recorded by gauge P7 for Event 2 and P8 for Events 1 and 2 were discarded because of excessive interferences emanating from the combined effects of boundary interference and / or gauge ringing (excessive noise).

Regression lines are shown as straight lines intercepting the axis. The effect of point scattering for Event 1 and 2 is most noticeable with infield and far-field gauges and is the main cause for the Event 1 and 2 gradients (α) diverging from the gradient of the standards TNT and pentolite. The dashed "line of best fit" is the result that can be anticipated from readings obtained under ideal conditions, i.e., from many PBXW-115 firings measured at a deep infinite boundary site.

A comparison of similitude constants α_θ and k_θ for PBXW-115 (Events 1 and 2), for PBXN-111 [15] and for various other high explosives is given in Table 7 (Section 4.7).

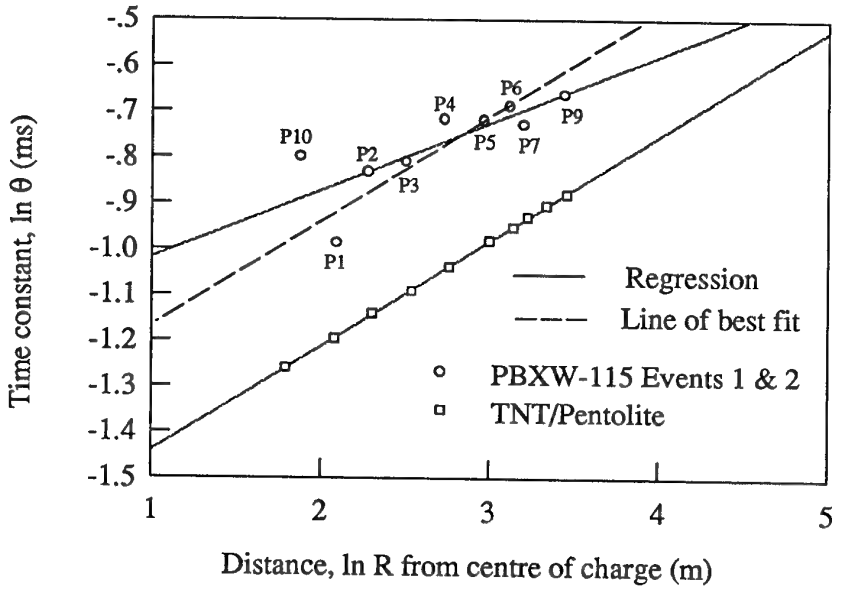

Figure 6:. Double ln plot of (a) θ versus R_n for TNT/pentolite and (b) θ versus R_c for PBXW-115 Events 1 and 2.

4.4 Peak Pressure

Peak pressures (P_m) were determined with the aid of a computer program [20] used for analysis and calibration of pressure versus time signals.

P_m is assigned to the initial highest pressure reading by this program. These P_m values are then assigned to their appropriate corrected gauge distance, R_c. Readings with excessive signal noise (due to shock wave reflections or poor gauge response) can introduce scatter in plotted P_m versus R results; for example, P_m recorded at gauge P7

for Event 2 could not be resolved because of excessive signal noise and was therefore discarded.

Double logarithmic plots of P_m versus R form straight lines with gradients of $-\alpha_P$ as defined in Section 4.3.1.

When results from PBXW-115 (Aust.) are compared with those from standard TNT and pentolite plots as in Figure 7, any anomalous P_m gauge readings are readily identified (P6, P8 and P9). It is interesting to note that, unlike the infield θ gauge response, the infield and mid-field P_m gauge responses for Event 1 and 2 are in line with the standard TNT and pentolite responses. The far-field gauges P8 and P9 gave the only anomalous gauge responses, indicating that some boundary reflection interference has probably taken place.

The regression gradient ($-\alpha_P$) of Events 1 and 2 which includes the far-field gauge responses is similar to the standard TNT and pentolite and becomes almost identical if one ignores the far-field gauge responses. Were PBXW-115 firings measured under ideal conditions, it would be anticipated that these far-field anomalies would disappear.

The P_m data used for creating the double log plots in Figure 7 is listed in Table 4. The α_P values for TNT, pentolite and PBXW-115 (Event 1 and 2) are also shown in Figure 7.

A comparison of similitude constants α_P and k_P thus derived from these data and from PBXN-111 [15] and other explosives are given later in this paper (Table 7, Section 4.7).

Table 4: P_m readings recorded at nominal (R_n) and corrected (R_c) distances from charge centre for 25 kg of TNT, Pentolite, PBXW-115 (Event 1, and 2).

Function			Peak pressure Pm			
			PBXW-115		TNT	Pentolite
Gauge	Distance m		Event 1	Event 2		
N°	R_n	R_c	MPa	MPa	MPa	MPa
P10	6.0	6.5	27.6	28.79	22.0	23.76
P1	8.0	8.1	21.0	21.42	16.0	17.28
P2	10.0	9.8	18.1	17.46	12.8	13.61
P3	12.6	12.2	13.0	13.78	10.0	10.7
P4	15.8	15.3	10.2	10.4	7.6	8.21
P5	20.0	19.4	7.8	7.82	5.8	6.3
P6	23.0	22.5	6.1	6.01	5.0	5.4
P7	25.0	24.5	6.2	-	4.5	4.86
P8	28.0	27.4	4.3	4.40	4.0	4.32
P9	31.6	31.1	6.0	5.14	3.55	3.83

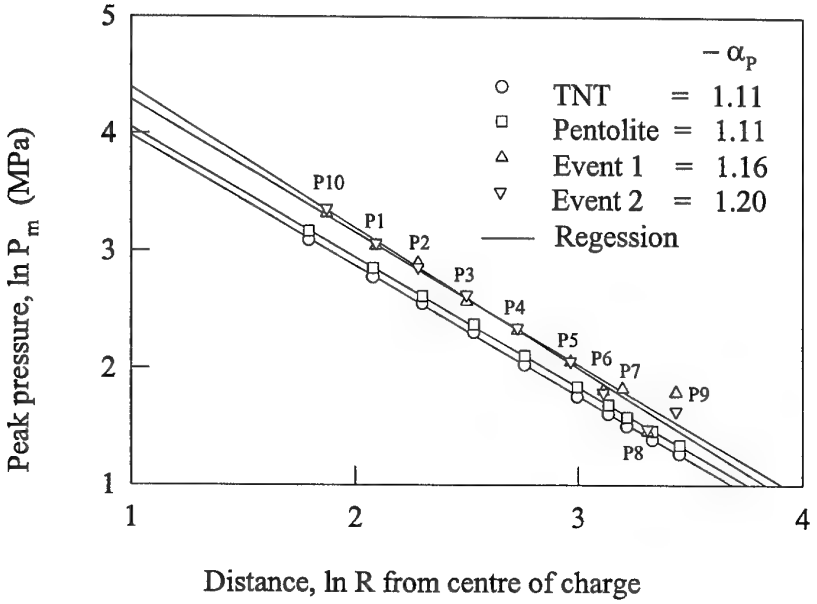

Figure 7: Double ln plot of (a) P_m versus R_n for TNT, (b) P_m versus R_n for pentolite and (c) P_m versus R_c for PBXW-115 (Event 1 and 2).

4.5 Impulse

The impulse of an explosion is defined as the time integral of pressure from time zero to time t. By definition, the impulse, I(t), of a shock wave front per unit area up to a time *t* is described by Equation 4

$$I(t) = \int_0^t P(t)\,dt \qquad (4)$$

where P(t) is the recorded pressure. P_0 is the base line pressure reading at t = 0. Normally P(t) - P_0 is used as the integrand but, in most cases, P(t) is so large compared with P_0 that the difference is of little importance [16]. The limiting value for t is usually taken as 5 x θ, although, in some analyses, a figure of 6.7 x θ is used.

In practice, boundary influences in confined water measurements invariably occur; as a result, this latter integration time range is seldom used. In addition, experience has also shown that the longer integration time adds little to the value of the area summed.

Double logarithmic plots of I versus R for standard cast TNT and pentolite form straight lines with gradients of - α_I as defined in Section 4.3.1. The plot of ln I versus ln R for PBXW-115, when compared with that of standard TNT or pentolite as shown in

Figure 8 again identifies anomalous responses from various gauges (P10, P1, P7, P8 and P9).

The first in-field gauge, P10, again appears to have a larger-than-expected response for reasons stated in Section 4.3.2. This large time constant (θ) response effectively increases the integration range of Equation 4 and hence computes a higher-than-anticipated value for impulse. A similar argument applies for the second in-field gauge P1, which gives a low θ response as explained in Section 4.3.2 ; here the correct integration range of Equation 4 is effectively reduced resulting in a lower-than-anticipated value for the calculated impulse at that location.

The obvious effect of anomalous θ determinations on the computed impulse values is that they will compound with P_m anomalies and increase the scatter of points in the linear ln I versus ln R relationship. Hence the deviations in computed impulse recorded by gauge P10 and P1 are primarily influenced by anomalies arising from computed values of θ, while deviations resulting from measurements at P8 and P9 arise from peak pressure (P_m) anomalies, which in turn have their origins in boundary effects. Errors in estimating the correct gauge position has a negligible effect on the scatter of points in the linear ln I versus ln R relationship.

The impulse data used for creating the plots in Figure 8 is listed in Table 5.

The α_I values for TNT, pentolite and PBXW-115 (Aust.) (Event 1 and 2) are also shown in Figure 8. A comparison of similitude constants α_I and k_I for PBXW-115 (Events 1 and 2), PBXN-111 [15] and various high explosives are given in Table 7 (Section 4.7).

Table 5: Impulse values calculated at nominal and corrected distances from charge centre for 25 kg of TNT, Pentolite, PBXW-115 (Event 1, and 2).

Function			Impulse I			
			PBXW-115		TNT	Pentolite
Gauge	Distance, m		Event 1	Event 2		
N°	R_n	R_c	kPa.s	kPa.s	kPa.s	kPa.s
P10	6.0	6.5	15.7-16.1	15.5 - 15.8	8.9	8.9
P1	8.0	8.1	8.7	8.4 - 8.5	6.8	6.8
P2	10.0	9.8	8.5 - 8.6	8.8 - 9.0	5.6	5.6
P3	12.6	12.2	6.6	6.9 - 7.2	4.5	4.5
P4	15.8	15.3	6.3 - 6.4	6.3 - 6.5	3.75	3.7
P5	20.0	19.4	4.7	4.5 - 4.7	3.0	3.0
P6	23.0	22.5	4.0 - 4.1	3.3 - 3.5	2.7	2.7
P7	25.0	24.5	2.5 - 3.7	2.5 - 3.1	2.45	2.45
P8	28.0	27.4	2.6	2.5 - 2.6	2.25	2.25
P9	31.6	31.1	3.4 - 3.5	3.3 - 3.4	2.00	2.05

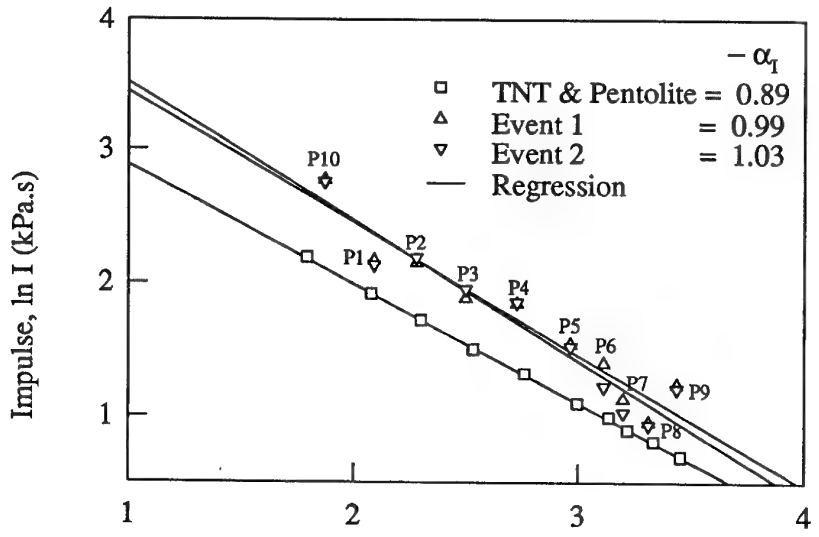

Figure 8: Double ln plot of (a) I versus R_n for TNT/Pentolite and (b) I versus R_c for PBXW-115 Event 1 & 2

4.6 Energy Flux Density

Energy flux density or energy flux (E) is another significant measure of the shock wave output [16]. Energy flux is determined from the integral of P^2 dt over the duration of 5 time constants.

$$\therefore \qquad E \qquad \propto \int_0^{5\theta} P^2\, dt \qquad (5)$$

where P is the recorded pressure. The energy flux density relationship of Equation 5 with the inclusion of the after flow correction [16, 19] becomes,

$$E = \frac{1}{\rho_0 C_0}\left(1 - 2.422\times10^{-4} P_m - 1.031\times10^{-8} P_m^2\right)\int_0^t P^2(t)dt \qquad (6)$$

where $\rho_0 C_0$ is the acoustic impedance of the medium, 5θ is the upper time limit, and P_m is peak pressure.

At a P_m of 140 MPa, the contribution from the corrections for the after flow (the two negative terms in Equation 6) amounts to 3.5% of total energy flux. At lower pressures of 30 MPa, as in this work on 25 kg charges of PBXW-115 (Aust.), the contribution from the after-flow to the total energy flux becomes insignificant.

Double logarithmic plots of E versus R for standard cast TNT and for pentolite form straight lines with gradients of α_E (Section 4.3.1).

These PBXW-115 energy flux plots when compared with that of standard TNT and pentolite (Fig. 9) again identifies anomalous gauge responses from the far-field gauges P8 and P9. It is noteworthy that the magnitude of scattering of the infield gauge response for computed E values at gauges P10 and P1 when compared with those from the far-field gauges P8 and P9, is less than it is for the impulse plots (Fig. 8).

The energy flux data used for creating the plots in Figure 9 is summarised in Table 6. These data enable one to determine the similitude constants α_E and k_E for PBXW-115 (Events 1 and 2) (Table 7, Section 4.7).

The α_E values for TNT, pentolite, PBXW-115 (Event 1 and 2) are also shown in Figure 9.

Table 6: Energy flux values calculated at nominal and corrected distances from charge centre for 25 kg of TNT, Pentolite, PBXW-115 Event 1, and 2.

Function			Energy Flux			
			PBXW-115		TNT	Pentolite
Gauge	Distance, m		Event 1	Event 2		
N°	R_n	R_c	E m.kPa	E m.kPa	E m.kPa	E m.kPa
P10	6.0	6.5	112 - 113	116.5-116.9	53.0	57.8
P1	8.0	8.1	54.3	53.4	29.5	32.2
P2	10.0	9.8	41.7	41.9 - 42.0	19.0	20.7
P3	12.6	12.2	23.7	24.9 - 25.1	11.9	13
P4	15.8	15.3	16.7 - 16.9	16.7 - 16.8	7.5	8.13
P5	20.0	19.4	9.4	9.1 - 9.2	4.6	5.01
P6	23.0	22.5	6.2 - 6.3	5.2 - 5.23	3.5	3.82
P7	25.0	24.5	4.1 - 5.9	4.4 - 5.5	2.9	3.16
P8	28.0	27.4	2.3	2.4 - 2.5	2.3	2.51
P9	31.6	31.1	4.8	4.5	1.8	1.96

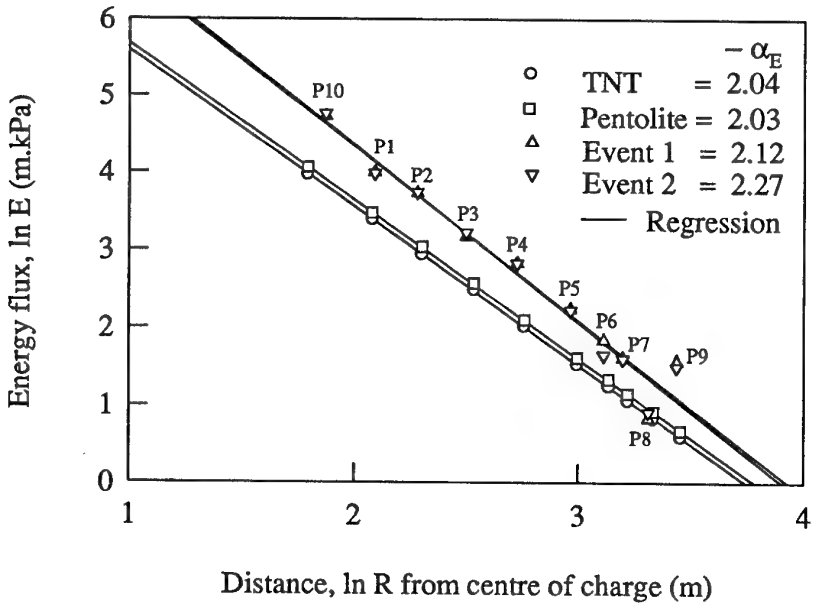

Figure 9 Double ln plot of (a) E versus R_n for TNT, (b) E versus R_n for pentolite and (c) E versus R_c for PBXW-115 Event 1& 2

4.7 Comparison of Similitude Constants and Coefficients

Table 7 summarises the various underwater explosion similitude constants and coefficients calculated for PBXW-115 (Events 1 and 2) from the experimental data presented in this report. The table also includes the corresponding parameters quoted for PBXN-111 and several other explosives.

Similitude constants are usually quoted for a given range of pressures; ie. there is a validity range, which is defined as the range of pressure (MPa) over which the equations apply and the data has been determined. To ascertain a complete validity range, an explosive should be assessed at increasing mass increments with extensive number of firings at each mass so that the pressure range over which the equations apply can be established with confidence [19].

Table 7: Similitude constants and coefficients for various high explosives

Parameter	Ref	$\theta/W^{1/3}$		P_m		$I/W^{1/3}$		$E/W^{1/3}$	
Explosive		k_θ	α_θ	k_P	α_P	k_I	α_I	k_E	α_E
TNT	19	0.084	-0.23	52.4	1.13	5.75	0.89	84.4	2.04
Pentolite	19	0.084	-0.23	56.5	1.14	5.73	0.91	92.0	2.04
H-6	19	0.088	-0.28	59.2	1.19	6.58	0.91	115.3	2.08
HBX-1	19	0.083	-0.29	56.7	1.15	6.42	0.85	106.2	2.00
Event 1		0.120	-0.18[a]	69±3	1.16	10±2	0.99	180	2.12
Event 2		0.109	-0.23[a]	72±3	1.20	10±2	1.03	210	2.27
Event 1 & 2		0.110	-0.21[b]	70.5	1.18	10	1.01	195	2.20
PBXN-111	15	0.101	-0.268	56.5	1.16	7.9	0.904	117	2.07

(a) readings from gauges P7 Event 1 and P8 Event 1 & 2 excluded
(b) combined α_θ = - 0.15 as shown in Figure 6 when readings from gauges P7 Event 1 and P8 (Event 1 & 2) are included

In this work the similitude constants for Australian made PBXW-115 (Event 1 and 2) were derived from limited data (two firings of 25 kg charges) and therefore the range over which these constants apply cannot be determined with any certainty. The validity range for both TNT and pentolite is 3.4 -138 MPa and, for HBX-1 it is 3.4 - 60 MPa [19]. It is reasonable to assume that, for PBXW-115 (Aust.), a similar validity range applies.

4.8 Shock Wave Energy

Shock wave energy (E_{SW}) is a function of energy flux,

$$E_{SW} = 4\pi R^2 E \qquad (7)$$

where E is the energy flux density or energy flux corresponding at a distance, R, from the centre of the exploded charge.

The calculated values of E_{SW} for PBXW-115 (Events 1 and 2) using Equation 7 are compared with those from TNT and pentolite (Tables 8 and 9). They are also reproduced in graphical form in Figure 10.

The results in Table 9 illustrate the validity of using the "Principle of Similarity for Shock Waves". In Table 9, the E_{SW} at the intercept for 50 kg TNT is 53 MJ and for 5 kg TNT it is 5.2 MJ. Therefore for a tenfold increase in explosive mass a tenfold increase in E_{SW} can be anticipated. However, the linear plot of E_{SW} versus R has a gradient with a slightly negative slope, indicating that a small amount of energy is lost (mainly through heating of water) as it traverses the water medium. Any discrepancy in assessing R or E correctly for PBXW-115 (Event 1 and Event 2) can be directly attributed to the relatively large scatter in the results obtained from the different gauges (Figure 10).

The erratic behaviour of the far-field gauge in Events 1 and 2 for PBXW-115 is again evident; the reason for this is that quarry boundary influences on the decaying primary shock wave have become more significant with increasing distance from the charge.

Table 8: Shock wave energy values calculated at nominal and corrected distances from charge centre for 25 kg of TNT, Pentolite, PBXW-115 Event 1, and 2.

Function			Shock wave energy			
			PBXW-115		TNT	Pentolite
Gauge	Distance m		Event 1	Event 2		
N°	R_n	R_c	MJ	MJ	MJ	MJ
P10	6.0	6.5	50.7-51.0	52.7-52.9	24.0	26.13
P1	8.0	8.1	43.6	43.0	23.7	25.86
P2	10.0	9.8	52.4	52.6 - 52.8	23.9	26.03
P3	12.6	12.2	47.3	49.7- 50.0	23.7	25.94
P4	15.8	15.3	52.5 - 52.9	52.4-52.7	23.5	25.49
P5	20.0	19.4	47.4	45.6 - 46.0	23.1	25.20
P6	23.0	22.5	41.5 - 41.8	39.6	23.3	25.36
P7	25.0	24.5	32.4 - 46.2	34.8 - 43.5	22.8	24.83
P8	28.0	27.4	22.8	23.6 - 24.6	22.7	24.70
P9	31.6	31.1	59.8 - 60.2	56.3-56.5	22.6	24.62

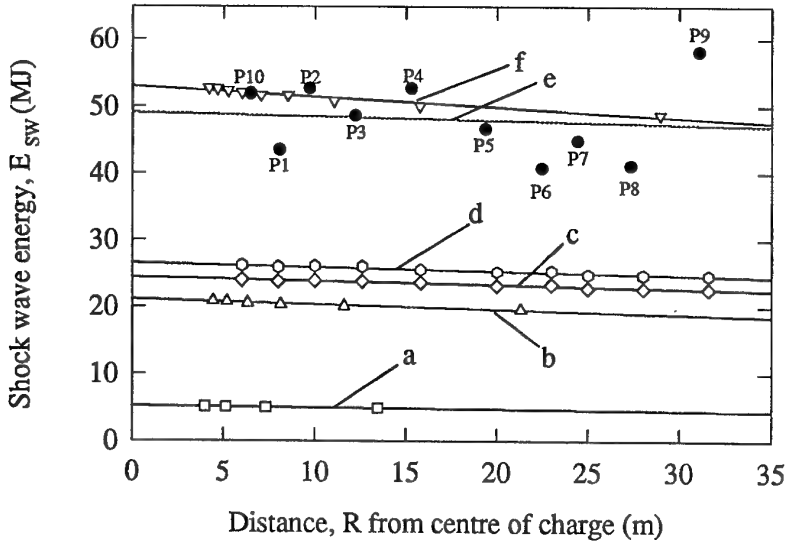

Figure 10: Linear plot of (a) E_{SW} versus R for 5 kg TNT, (b) E_{SW} versus R for 20 kg TNT, (c) E_{SW} versus R_n for 25 kg TNT, (d) E_{SW} versus R_n for 25 kg pentolite, (e) E_{SW} versus R_c for PBXW-115 Event 1 and 2 combined and (f) E_{SW} versus R_n for 50 kg TNT

Table 9: Summary of E_{SW} versus R plot data used in Figure 10

Plot	Explosive	Mass (kg)	Gradient	Intercept
a	TNT	5	-0.03	5.2
b	TNT	20	-0.07	21.0
c	TNT	25	-0.06	24.4
d	Pentolite	25	-0.06	26.5
e	PBXW-115	25	-0.06	49.0
f	TNT	50	-0.16	53.0

4.9 Shock Factor

Shock factor (SF) is used to assess target response against the effects of an incident shock wave. It is a measure of a target's ability to withstand various threshold levels of damage from exposure to increasing levels of shock over a range of stand-off distances [21]. The shock generated by an explosive source is related to an equivalent mass of TNT. The empirically derived shock factor relationship is dependent on explosive mass and stand-off distance and is defined by Equation 8

$$SF = \frac{\sqrt[n]{W_{TNT}}}{D_1} \qquad (8)$$

where W_{TNT} is mass of explosive TNT equivalent (kg), n is approximately 2 and D_1 is the distance from explosive to the closest point on the target. From the data presented in Fig 10, PBXW-115 would be expected to be 40% more effective than TNT on a mass basis, in inflicting damage to potential targets. This claim assumes that the effectiveness of an explosive is directly proportional to SF; an assumption which, in practice, is not always true.

5. Bubble Parameters

The major effects of the bubble generated from an underwater explosive event take place over a much larger time frame than that of the shock wave. The bubble parameters used in assessing the effects and behaviour of the expanding combustion products are relative bubble energy (E_{RB}), maximum bubble radius (A_m) and bubble rise after each oscillation (Z_i).

5.1 Relative Bubble Energy

Relative bubble energy (E_{RB}) reflects the amount of work done by the expanding combustion products. It is derived from the first bubble period constant (K) and is defined by Equation 9

$$E_{RB} = \left(K_{exp.} / K_{ref.} \right)^3 \qquad (9)$$

where $K_{exp.}$ is the bubble period constant (as defined later, in Section 5.3) for the explosive under test and $K_{ref.}$ is that for TNT or pentolite [16, 19].

5.2 Bubble Period

The first bubble period (T) is the time interval between the arrival of the first incident shock and the first acoustic shock generated by the hydrostatic pressure compression of the combustion products to the first minimum as shown in Figure 11.

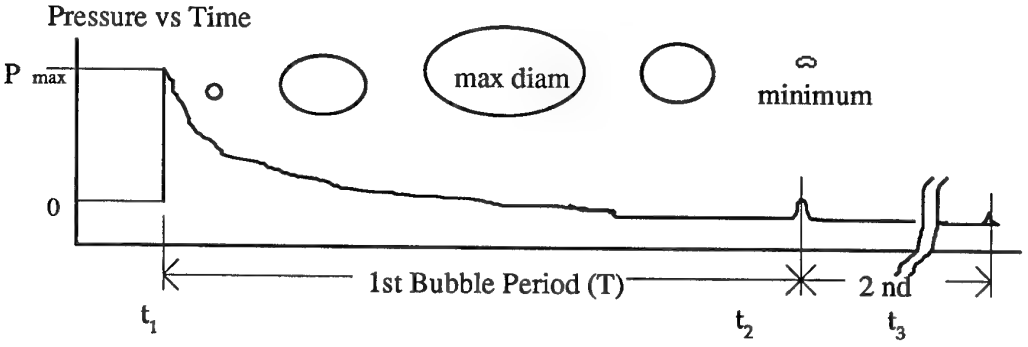

Figure 11: Pressure time recording reflecting the incident peak pressure decay over the first and second bubble periods.

The data from the experimental records used to determine the first bubble period for PBXW-115 are listed in Tables 10 and 11.

The variation in the first bubble period for Events 1 and 2 is less than 0.3% when noisy signals are omitted. Noisy signals were also omitted in arriving at the average bubble period for each event.

In both events, the nearest pressure gauge (P10) registered a second bubble period of 0.51 seconds. However, on the remaining gauges, the second bubble period signals

could not be identified above background noise levels. The bubble period is used to calculate the bubble period constant.

Table 10: Bubble Period Data for Event 1

Gauge N°	R_n m	R_c m	time, t_2 s	time, t_1 s	$t_2 - t_1$ T, s
P10	6.0	6.5	0.723	0.0713	0.652
P1	8.0	8.1	0.738	0.0881	0.650
P2	10.0	9.8	0.738	0.0894	0.649
P3	12.6	12.2	0.737	0.0881	0.649
P4	15.8	15.3	0.738	0.0902	0.648
P5	20.0	19.4	0.736	0.0880	0.648
P6	23.0	22.5	0.738	0.0901	0.648
P7	25.0	24.5	0.737	0.0880	0.649
P8 (noisy signal)	28.0	27.4	0.732 - 0.743	0.090	0.642 - 0.653
P9	31.6	31.1	0.740	0.088	0.652

T average = 0.649 ± 0.002 s
R_n nominal displacement of gauge from charge
R_c corrected R_n

Table 11: Bubble Period Data for Event 2

Gauge N°	R_n m	R_c m	time, t_2 s	time, t_1 s	$t_2 - t_1$ T, s
P10	6.0	6.5	0.738	0.088	0.650
P1	8.0	8.1	0.739	0.089	0.650
P2	10.0	9.7	0.738	0.088	0.650
P3	12.6	12.2	0.739	0.090	0.649
P4 noisy	15.8	15.3	0.747	0.099	0.648
P5	20.0	19.4	0.751	0.101	0.650
P6	23.0	22.5	0.754	0.103	0.651
P7 very noisy	25.0	24.4	-	-	0.65
P8	28.0	27.3	0.756	0.106	0.650
P9	31.6	31.1	0.759	0.109	0.650

T average = 0.650 ± 0.002 s

5.3 Bubble Period Constant

The bubble period constant [16,19] of a bubble generated by an underwater explosion in free water is defined by Equation 10,

$$K = T \left(\frac{Z^{\frac{5}{6}}}{W^{\frac{1}{3}}} \right) \qquad (10)$$

where K is the bubble period constant (s. $m^{5/6}/kg^{1/3}$),

T is the first bubble period (s),

W is the charge mass (kg),

Z is the sum of the hydrostatic pressure at the charge depth, H, in units of m of water and the atmospheric pressure, H_0, units of m of water (approximately H + 10).

Equation 10 relates the bubble period constant, K, and the bubble period for free water explosions, T, to the depth and to the mass of the charge. This relationship, which has an empirical basis, really applies where the bubble is not closer than about 10 bubble radii to either the surface or bottom. This is not the case at the AMRLs Underwater Explosive Test Facility at Epping.

In cases where either the surface, the bottom, or both begin to influence the bubble one can use a quadratic correction equation to relate K and T following Swisdak [19]. This correction is defined by Equation 11, thus:-

$$\frac{0{\cdot}651\ \phi(y) W^{\frac{1}{3}}}{DZ^{\frac{1}{3}}} K^2 - K + \frac{T Z^{\frac{5}{6}}}{W^{\frac{1}{3}}} = 0 \qquad (11)$$

where D is the total water depth (m),

y equals H/D,

Z is the sum of the hydrostatic pressure at the charge depth, H, in units of m of water, and the atmospheric pressure, H_0, units of m of water.

For the Epping Quarry, we find y = 0.5 and from Swisdak [19, p. 66, Figure 10] we obtain $\phi(y) = 0.83$.

This leads to values for $K_{exp.}$ of 2.757 and 2.766 for PBXW-115 (Aust) (Events 1 and 2).

By applying these bubble period constants to Equation 9 we obtain an E_{RB} of 2.24 for Event 1 and an E_{RB}, of 2.25 for Event 2. This relative bubble energy is approximately 12% higher than that quoted by Connor for PBXN-111, the US navy equivalent of PBXW-115 (Aust.) [15].

The charge booster configuration used by Connor is different to that used at AMRL. The AMRL configuration [9] has a smaller centrally placed booster, that is

generally recognised as being more efficient upon initiation than the larger end initiated booster arrangement used by Connor at the Naval Surface Weapons Center, in 1985. A similarly higher value for relative bubble energy of H-6 (an aluminised RDX/TNT explosive) has also been found by David Jones of AMRL, Maribyrnong [22] using the same centrally placed booster configuration as in this work.

The booster main charge ratio we used was 1:50 compared to 1:100 for the Jones configuration and 1:13 for the Connor configuration. The implication of this will be addressed later.

5.4 Maximum Bubble Radius

To reduce damage to the pressure gauges, it is important to know - or, at least, to estimate - in advance the size of the maximum bubble radius so that infield gauges are not placed within the turbulent boundary of the expanding bubble. It is also important to set the charge at a depth, far in excess of the maximum bubble radius, in order to prevent premature venting of the first bubble maximum.

Swisdak estimated the maximum bubble radius with Equation 12

$$A_m = J \left(\frac{W}{Z}\right)^{1/3} \qquad (12)$$

where A_m is the maximum bubble radius (m),

J is the bubble radius coefficient, which depends on the explosive [19, p. 63-67]), and

Z is the sum of the hydrostatic pressure at the charge depth, H, in units of m of water, and the atmospheric pressure, H_o, units of m of water.

The value of J could not be determined directly for PBXW-115 and Bjarnholts [23] empirical relationship (13) relating the heat of explosion/detonation to an approximation of maximum bubble radius was used to estimate A_m. This relationship can be expressed in various forms, all of which are equivalent,

$$A_m \approx \left(\frac{1{\cdot}3\,QW}{1+H/10}\right)^{1/3} \text{ or } \left(\frac{13\,QW}{H+H_o}\right)^{1/3} \text{ or } \left(\frac{13\,QW}{Z}\right)^{1/3} \qquad (13)$$

where Q is the heat of explosion/detonation (MJ/kg),

W is the mass of explosive (kg),

H is the sum of the hydrostatic pressure at the charge depth, H, in units of m of water, and the atmospheric pressure, H_o, units of m of water.

The dimensions of A_m in Equation 13 do not equate with those of Q, W and Z as a result of being simplified from a more explicit expression found in Cole [16, p. 342].

The best approximation is obtained when the charge depth is two-thirds of the

distance to the bottom where corrections for the opposing effects of the surface and bottom boundaries cancel. By using the Cichra and Doherty [24] factor-analysis method of estimating the performance of underwater explosives we can arrive at a value for Q and hence obtain an approximation for A_m. Using the Cichra-Doherty H_2O-CO_2 "arbitrary" to calculate Q, the heat of explosion under Chapman-Jouguet conditions, Q for PBXW-115 was estimated to be in the range of 6.3 - 7.8 MJ/kg.

At Epping Quarry using 25 kg of PBXW-115 explosive A_m was calculated to be in the range of 4.8 - 5.2 metres at 8 m depth. This range for A_m was also in agreement with that estimated from the nomograph presented by Swisdak relating H, T and TNT mass equivalence to A_m. The nomographic confirmation was made possible after firing a PBX charge at a known depth; from this event, one was able to obtain a bubble period for PBXW-115 and relate this period to A_m and a TNT mass equivalence. The TNT mass equivalent using the nomograph also compares favourably with the directly measured PBXW-115 value for E_{RB} - derived TNT equivalents.

On the basis of the initial A_m estimate, the nearest pressure gauge was set at 6 m from the charge a distance expected at the time, to be well outside the limits of the disruptive effects of the first bubble maximum.

5.5 Bubble Motion

It is desirable to establish the number of bubble oscillations that are expected to occur before the bubble reaches the surface. If venting occurs before one complete oscillation takes place, then bubble period measurements are of doubtful value.

The position of the source of the bubble pulse can be establishes by estimating the displacement of the bubble at the time of the first minimum. Swisdak [19, pp. 71-74] relates bubble oscillations to TNT mass equivalents for underwater explosions where bottom influences are absent. Because of the potential bottom influences that exist at the quarry test site a reasonable estimate for the number of bubble oscillations before venting occurred could not be made with confidence. However, with a 25 kg PBXW-115 charge, assuming that bottom influences are minimal, the Swisdak approach indicated that 1.45 bubble oscillations were possible at an 8 metre firing depth when a TNT-equivalent reduced charge depth of 2.1 $m/kg^{1/3}$ is used. This reduced charge depth [19, p. 71] is obtained by using Equation 14,

$$Z_R = H/\sqrt[3]{W_{TNT}} \qquad (14)$$

where Z_R is the reduced charge depth in $m/kg^{1/3}$,

H is the charge depth in metres and

W_{TNT} is the TNT equivalent mass of explosive.

The TNT equivalent mass for 25 kg of PBXW-115 is 56.25 kg ($W_{PBX} \times E_{RB} = 25 \times 2.25$).

Sattler and Girnus [25] used the relationship expressed by Equation 15 to estimate the gas bubble rise for TNT equivalent mass of explosive after each successive bubble contraction to a minima,

$$Z_i = 12\,(2i-1)\,\frac{\sqrt{W_{TNT}}}{D_i + 10} \qquad (15)$$

Here, W_{TNT} is equivalent TNT explosive mass, D_i is ignition depth, i is the number of minima and Z_i is the rise in metres of the bubble centre after the i^{th} acoustic shock. This approximation does not appear to make any allowances for the surface repulsive effect that retards the rising bubble.

Equation 15 predicts that the first minima rise Z_1 is 5 metres; this means that, in the Epping Quarry, the bubble will be positioned at 3 m below the surface, when this occurs.

The second minima rise Z_2 is calculated to occur at 15 m; this is too large a value to be accommodated in the Epping Quarry, so any recorded second acoustic shock attributed to the bubble should be ascribed to a "partially vented bubble".

A_m was estimated to be 5 m and when the repulsive effect of the surface on the bubble is taken into consideration, A_m is expected to reach this value at a rise distance less than one-half Z_1.

The bubble is known to have a kidney shape at or near its first minimum [16, p. 279-80]. It is also known that the approximation of sphericity is least valid when the bubble reaches A_m near the free surface; here, local variations in hydrostatic pressure over the bubble boundary are much greater [16] and mathematical modeling suggests that, at A_m, it is reasonable to expect the horizontal diameter to be larger than the vertical diameter [19]. Be that as it may, if one takes the extreme case and assumes that the bubble is spherical at A_m, then, more than half a meter of water remains between the top of the bubble and the surface during the time leading to the first bubble pulse. On this basis alone, it can be seen that insufficient bubble migration has taken place for any bubble venting to occur during the first bubble period cycle.

The second bubble period cycle is not important in explosive assessment and any observable measurement made in view of the calculated second minima rise of 15 m (7m more than the available water head) would include some effects of venting.

In summary, both approaches predict that only one full bubble cycle is possible for 25 kg charges of PBXW-115 (Aust.) in the Epping Quarry site.

5.6 Pressure Gauge Positions

Originally the gauges were set at nominal distances (R_n) of 6, 8, 10, 12.6, 15.8, 20, 25, 28, and 31.6 metres from the point of detonation. The water filled quarry test site is sheltered by a peripheral ridge and does not suffer from the effects of currents or wave motion as do open ocean sites. However, the setting of the nominal gauge positions is known to change between successive events because of changes in the tension in the steel cables. which support the test array. Hence, some method of establishing the true position of the gauges for each event is required.

Measurements from the point of detonation (charge centre) of the time taken for the shock wave to arrive at each gauge (time of arrival technique) multiplied by the acoustic water velocity is known to give a gauge location that is reliable to ± 1%. The

time interval between a fibre optic transmitted signal emanating from the water /explosive interface and the arrival of the shock wave - generated signal emanating from the various pressure gauges is recorded as the time of arrival. The decay of the velocity of the shock wave (supersonic) as it passes the water/explosive interface to that of acoustic velocity takes place over a very short distance and is just compensated by the delay in ignition between the detonator and charge surface. Therefore corrections to allow for this decay in velocity are not necessary. The time of arrival relationship with position of gauges is now defined by Equation 16

$$R_c = C_w\ t \qquad (16)$$

where R_c is the corrected gauge position in metres taken from the centre of the charge
C_w is the acoustic water velocity based on temperature and salinity (1473 m/s for Epping Quarry) and
t is the time of arrival measured in seconds.

Corrected gauge distances are shown as R_c in tables 3, 4, 8 and 9.

6. Discussion of Results

6.1 Explosive Performance Differences of PBXW-115/PBXN-111

Both Australian-made PBXW-115 [8, 10, 11] and its US counterpart PBXN-111 [1, 2, 14, 15] are made from nominally identical molecular ingredients in the same proportions; hence, one would expect that their respective explosive energy outputs, which are determined solely by their thermochemical contents, would be identical. For this reason, one would expect that the large-scale explosive performance properties of PBXW-115 (Aust.) and PBXN-111 would be the same.

From the data presented in Tables 7, 8 and 12, it has been found that there are apparent major differences in the measured underwater explosive performance parameters of PBXW-115 (Aust.) and of PBXN-111. The author believes that the differences arise from the way these experiments were carried out - not because of subtle differences in the formulations, per se.

Differences in RDX crystal morphology, type and particle size are known to affect explosive properties [2, 10, 11] and these effects become noticeable when charge dimensions are below the minimum requirement necessary for maintaining maximum velocity of detonation (V of D_{max}) [11]. However in this work a right cylinder of 25 kg PBXW-115 (Aust.) was used. With the confining effect that the 8 meter water pressure head has, it is reasonable to assume that limiting V of D_{max} conditions have been maintained [11] and that any influence that RDX crystal morphology, type and particle size distribution may have on shock wave energy output has become negligible [9, 11].

Table 12: Comparison of Relative E_{SW} and E_{RB} of PBXW-115 (Aust), PBXN-111 (USA), H-6, TNT and Pentolite on an Equivalent Mass Basis.

Explosive	Relative E_{SW}	E_{RB}
PBXW-115 (Aust)	1.85	2.25
PBXN-111 (USA)	1.34	2.00
PBXW-115 (Calculated)[a]	1.22[b]	2.26
H-6[c]	1.18	1.54
Pentolite Standard[c]	1.00	1.00
TNT[c]	0.84	0.94

a) Cichra and Doherty [24] factor-analysis method for Q = 7.8 MJ/kg
b) Imput data for calculating E_{SW} is derived from underwater performance of ideal explosives and does not relate well to non ideal explosives such as PBXW-115.
c) Data obtained from non boostered systems.

6.2 Charge Design/Configuration

The importance of charge design in relation to booster size and the location of the boosters particularly with insensitive explosives such as PBXW-115 has been presented in an earlier report [9]. The effect that charge design has on relative shock wave energy, E_{SW}, and the relative bubble energy, E_{RB}, will be explained in Sections 6.2.1 and 6.2.2.

6.2.1 Effect on Shock Wave Energy Output

The main differences that exist between the AMRL charge configuration and that used by Connor are booster size and location. At AMRL a small centrally placed booster amounting to 2% of the total charge mass was used. Connor used a charge configuration with a large conical shaped booster located at the base of a right cylinder main charge; the mass of his booster amounted to 7.7% of the total charge mass.

Pentolite on an equivalent mass basis has a lower relative shock wave energy (1.00) than either PBXN-111 (Connor's figure, 1.34) or PBXW-115 (this work 1.85 ± 0.15 with anomalous readings, P7 and P8 ommited). An increase in size of the pentolite booster in relation to the main charge must therefore reduce the apparent overall shock wave energy output of the system and this may explain, in part, the discrepancy in the lower relative E_{SW} reported for PBXN-111.

The results reported by Connor for PBXN-111 represent those from a 29.5 kg (65 lb) system made up of 92.3% (≈ 92%) PBX and 7.7 % (≈ 8%) pentolite (by mass). Those described herein represent those from a system 98% PBX and 2% pentolite booster. The output per unit mass in this case should be expected to be greater than that from Connors work.

That is not all, however. One must consider the effects of booster location. Cole has shown that when boosters of mass in excess of 1% of the mass of the main charge are

located at the end of a cylinder, they can produce directional effects [16]. These directional effects may increase or decrease the overall shock wave energy output depending on whether the shock wave is measured at either the off-side, the detonator or far ends [16]. A satisfactory way of minimising the directional effects is to place the booster in a central location as opposed to a peripheral location. Any directional effects related to booster location are thereby negated.

6.2.2 Effect on Relative Bubble Energy (E_{RB})

The E_{RB} is essentially a measure of the amount of work that is done by the expanding combustion products [16, 19, 26]. Any process that contributes to the amount of expandable combustion material and / or increases its reaction temperature will enhance the E_{RB}. In principle, the combustible ingredients used in formulating PBXW-115 (Aust) and PBXN-111 are the same. Hence, the E_{RB} should be the same for each of these compositions. However, the E_{RB} obtained for PBXW-115 (Aust.) in this work is some 12.5% higher than that reported for PBXW-115 (USA) by Connor (Table 12). It is therefore reasonable to suggest that the difference in measured E_{RB} values may again be due to differences in charge design.

It is known that finely divided aluminium when added to explosives increases the temperature of the expanding combustion gases by reacting exothermically with them and that this reaction takes place well after the shock wave has been generated. The use of a smaller non aluminised booster as in this work effectively increases total aluminium content of the combined main charge booster system and therefore extends the exothermic reactions that are the prime component of E_{RB}.

A minor contribution can be expected from the more efficient interaction of non aluminised combustion products generated by the centrally located booster. These combustion products are totally enveloped by the alumunised PBX and are likely to have a greater interaction with the main charge aluminium than those located peripherally as in Connors work. The outcome of the higher overall aluminium content and more efficient interaction is that more of the available amount of work done is maximised. The increase in observed relative bubble energy output (E_{RB}) is a direct result of this.

6.3 Effect of Charge Size on Performance

The charge size used by Connor was 27.2 kg; that used here was 25 kg. Such a small variation in charge size is considered to have an insignificant effect on either shock wave energy or E_{RB}. However larger charges of say 200-300 kg mass are expected to show a slight increase in E_{RB} because an improved efficiency in reaction between fuels and oxidants within the expanding combustion products should occur. Increased conservation of generated heat would also contribute to a higher E_{RB}.

To support this suggestion, Sattler and Girnus [25] have reported on the underwater performance of a 50 kg explosive charge, of density 1.83 Mgm^{-3}, based on 45% AP, 18% RDX and 27% Al overcast with 10% SSMTR 8870 (a German explosive

equivalent to H-6). They found that this material has a high E_{RB} of 2.32 (relative to TNT). As this composition is not too dissimilar to that of PBX-115, one could argue that the increase in E_{RB} may not be entirely due to the higher Al content but rather to the increase in charge size.

6.4 Suitability for Mine Neutralisation

Experiments show that sympathetic detonations in explosive materials can be initiated underwater by an underwater shock wave [27, 28]. Chung has demonstrated that, in order to initiate explosive materials by an underwater shock wave, one requires a low, sustained pressure, rather than a short-lived intense pulse [29]. A feature of a sustained pressure pulse is that it has a long time constant. PBXW-115 has a low velocity of detonation (when compared to TNT or pentolite) but a large power output and hence readily produces the ideal low sustained pressure conditions as specified by Chung.

Further experiments are required to determine the critical detonation conditions needed for PBXW-115 - initiated sympathetic detonations underwater.

7. Conclusion/Recommendations

The use of AMRL Epping Quarry site as a test venue for this work was found to be adequate. However, if underwater explosive performance assessment is required for larger sized charges than those described here (mass: 25 kg), then these will need to be conducted in deeper waters, preferably where boundary effects will be minimised.

Although apparent differences in the underwater explosive performance data have been found for PBXW-115 (Aust.) and its qualified US counterpart PBXN-111, it is likely that they are an artifact of the different experimental methodologies, both in the choice of booster mass and its location with respect to the bulk of the main charge. For optimum underwater explosive performance assessment, it is recommended that booster size be kept at proportions of 1% of main charge size and that it be placed centrally. Main charge sizes particularly when dealing with insensitive explosives should be sufficiently large to ensure that maximum velocity of detonation conditions are being observed.

Similitude equation constants used for predicting performance behaviour of large masses of PBXW-115 explosive have been determined (Table 7) and the relative shock wave energy and relative bubble energy outputs of Australian-made PBXW-115 have been determined (Table 12). It is apparent that these two parameters are greater than the corresponding parameters of Composition H-6, a widely used underwater explosive, and that, on performance grounds, PBXW-115 deserves to be investigated more fully for service applications.

The suitability of PBXW-115 (Aust) as an alternative fill to PBXN-103 for a warhead like the Mark 46 torpedo warhead based on the improved underwater performance data from this work is now a possibility worth investigating.

8. Acknowledgments

The author gratefully acknowledges the assistance of several colleagues in the preparation of material contained in this report, in particular Dan Whelan, who has read many versions of this and related manuscripts and made many excellent suggestions as to its final form. David Jones and Michael Chung are thanked for many helpful discussions on aspects of interpreting and reporting data. George Yiannakopoulos and Andrew Krelle (Ship Structures and Materials Division, AMRL), who advised and participated in the underwater firings program. Les Heathcote, Max Joiner and Robert Hughes are thanked for their efforts expended on machining the large PBX discs. Special thanks are given to Mick Chick for support during difficult stages that were encountered in the course of planning this work.

9. Nomenclature

A_m	Maximum gas bubble radius [m]
a	Similitude constant
a_x	Similitude constant for parameter x = θ, P_m, I or E
C_W	Sound velocity in water [m/s]
D	Total water depth [m]
D_1	Distance from charge to closest point on target [m]
E	Energy flux [m.Pa]
E_{RR}	Relative bubble energy [a ratio relative to pentolite]
E_{SW}	Shock wave energy [J]
H	Charge depth [m]
H_O	Atmospheric pressure head depth equivalent [m]
I	Impulse [Pa.s]
K	Bubble period constant [$s.m^{5/6}/kg^{1/3}$]
$K_{exp.}$	Bubble period constant for explosive under test [$s.m^{5/6}/kg^{1/3}$]
$K_{ref.}$	Bubble period constant for TNT or pentolite (2.11 $s.m^{5/6}/kg^{1/3}$)
k	Similitude constant
k_x	Similitude constant for parameters x = θ, P_m, I or E
$\phi(y)$	Boundary effect correction factor
θ	Time constant [μs]
P	Pressure [MPa]
P_m	Peak pressure [MPa]
Q	Heat of explosion [MJ/kg]
R	Gauge distance from the charge [m]
R_n	Nominal gauge distance [m]
R_c	Corrected gauge distance [m]
T	First bubble period [s]
t	Time [s]
V of D_{max}	Velocity of Detonation at infinite diameter
W	Charge mass [kg]
y	Charge depth/Total depth ratio
Z	Hydrostatic pressure [m]
Z_i	Rise in metres after the i^{th} acoustic shock (i = 1, 2, ...) [m]
Z_R	Reduced charge depth [$m/kg^{1/3}$]

10. References

1. Anderson, E.W. and Leahy, J.F. 1985.
"*Qualification Testing of PBXW-115*" (U) Naval Surface Weapons Center, White Oak, Maryland, USA) Technical Report, NSWC TR 85-298 (Confidential).

2. Forbes, J.W., Lemar, E.R., Sutherland, G.T., and Baker, R.N., 1992.
"*Detonation Wave Curvature, Corner Turning and Unreacted Hugoniot of PBXN-111*", Naval Surface Warfare Center (Maryland, USA) Technical Report, NSWC-TR-92-164.

3. USN Insensitive Munitions Office, 1994.
Navy Sea Systems Command, Advanced Development FY 95 Program Overview.
Section II.

4. Richardson, Barry, Defence Research Agency, Fort Halstead, Kent, UK, 1994.
Private conversation with the author, Melbourne, November, 1994.

5. Wanninger, P., 1991.
22nd International Annual Conference of ICT, 1991, Paper 5, "Empfindlichkeit von Explosivstoffen und Ladungen gegen Beschuss", esp. p 23.

6. Held, M., 1992.
"Steady Detonation Velocity of Infinite Radius derived from Small Samples", Propellants, Explosives and Pyrotechnics, **17** 275-277.

7. Watts, A.J. (Editor), 1994
Jane's Underwater Warfare Systems, 1994/95. Sixth Edition.

8. Bocksteiner, G. and Billon, H. R., 1991
Insensitive Polymer Bonded Main Charge Explosive PBXW-115: Binder and Formulation Studies (MRL Technical Report, MRL TR 91-54).

9. Bocksteiner, G., 1994
"*A Novel Technique for the Preparation of Centrally Boostered Cast Cured PBX Charges*" Defence Science Technology Organisation, AMRL, Technical Report DSTO- TR-0040

10. Bocksteiner, G. and Whelan, D.J. 1993
"*A Comparison of the Explosive Properties and Performance of Underwater Explosives, PBXW-115 (Aust), PBXW-115 (USA) / PBXN-111, Composition H-6 and Torpex 4D/TF*", Materials Research Laboratories Technical Report, MRL-TR-93-45 (Restricted)

11. Bocksteiner, G. Wolfson, M.G. and Whelan, D.J. 1994
"The Critical Diameter, Detonation Velocity and Shock Sensitiveness of Australian-made PBXW-115", Defence Science Technology Organisation, AMRL, Technical Report DSTO-TR-0076

12. Bocksteiner, G. and Whelan, D.J. 1995
"The Effect of Ageing on PBXW-115 (Aust.), PBXN-103 and PBXN-105" Defence Science and Technology Organisation (DSTO) Technical Report, DSTO-TR-0228

13. Australian Ordnance Council, HQADF, 1995.
Plastic Bonded Explosive: PBXW-115 (Aust.), Advice on Qualification for Service, AOC Report No. AOC-204.95 (13 June 1995).

14. Forbes, J.W., Lemar, E.R. and Baker, R.N. 1989.
"Detonation wave propagation in PBXW-115", Ninth Symposium International on Detonation, Portland, Oregon, USA, Aug-Sept. 1989, Proceedings, pp 846-854.

15. Connor, J.G., 1984.
"Underwater Explosion Effectiveness of PBXW-113, PBXW-114 and PBXW-115", Naval Surface Weapons Center Technical Report, NSWC-TR 84-396.

16. Cole, R.H., 1948
"Underwater Explosions", Princeton University Press, Princeton, New Jersey, USA.

17. Encyclopedia of Explosives and Related Items, 1983.
US Armament Research and Development Command, Large Calibre Weapons System Laboratory (Dover, NJ, USA), PATR 2700 Vol. 10 (1983), Underwater Measuring Techniques, pp U 38-81.

18. Hicks, A.N., 1976
"Optimisation of Explosives for use Underwater" Sixth Symposium (International) on Detonation, San Diego, California, USA, Aug. 1976, Proceedings, pp 550-560.

19. Swisdak M.M., 1978
"Explosion Effects and Properties: Part II- Explosion Effects in Water", Naval Surface Warfare Center Technical Report, NSWC/NOL TR 76-116

20. Krelle, A.J.W. and Wiese, D. 1992
Blast, a computer program written in Ship Structures and Materials Division, AMRL, for analysis of underwater blast parameters.

21. Bishop, J.H., 1993
"Underwater Shock Standards and Tests for Naval Vessels" Proceedings of the

Institution of Engineers Australia, Dynamic Loading in Manufacturing and Service Conference, 9-11 Feb. Melbourne Australia, pp 157-163.

22. Jones, D.A. and Northeast, E., 1995.
"*Effects of Case Thickness on the Performance of Underwater Mines*", Defence Science Technology Organisation, AMRL, Technical Report DSTO- TR-0120.

23. Bjarnholt, G., 1980
"Suggestions on Standards for Measurement and Data Evaluation in the Underwater Explosion Test" Propellants and Explosives, **5** pp 67-74.

24. Cichra, D.A. and Doherty, R.M. 1989.
"*Estimation of Performance of Underwater Explosives*", Ninth International Symposium on Detonation, Portland, Oregon, USA, Aug-Sept 1989, Proceedings, pp 633-639.

25. Sattler and Girnus, 1980-81. Bocksteiner, G. \Translator 1988.
"*Wirkung von Unterwassersprengstoffe in See*", (Action of Underwater Explosives in Seawater), Underwater explosive tests conducted by the German Bundeswehr at Erprobungstelle 71 Schonhagen/Kiel. MRL-TT-0009

26. Bjarnholt, G. and Holmberg, R. 1976
"*Explosive Expansion Work in Underwater Detonations*", Sixth Symposium (International) on Detonation, San Diego, California, USA, Aug. 1976, Proceedings, pp 540-550.

27. Chung, M.J., McQueen, D. and McVay, L., 1994
Initiation of Detonations in Composition B by an Underwater Shock Wave. AMRL Technical Report in Course of Publication (AMRL File G9 4/8-4705)

28. Chung, M.J. and Kinsey, T., 1995
A Study of Underwater Blast Effects on Simple Structures, Shielded and Bare Explosive Materials, Paper Submitted to the 4th International Symposium on the Behaviour of Dense Media Under High Dynamic Pressures Tours France

29. Chung, M.J., 1994
Investigation of Critical Initiation Parameters of Underwater Shock Waves used to Dispose of Sea Mines, TTCP Sub Group G Symposium on Mine Counter Measures and Mine Disposal, Edinburgh United Kingdom

Evaluation of Underwater Explosive Performance of PBXW-115 (AUST)

G. Bocksteiner

AUSTRALIA

1. DEFENCE ORGANISATION

a. Task sponsor: DARMENG-N

b. S&T Program

Chief Defence Scientist
FAS Science Policy
AS Science and Industry Interaction
AS Science Corporate Management
} shared copy

Counsellor Defence Science, London (Doc Data Sheet)
Counsellor Defence Science, Washington
Scientific Adviser to Thailand MRDC (Doc Data Sheet)
Senior Defence Scientific Adviser/Scientific Adviser Policy and Command (shared copy)
Navy Scientific Adviser
Scientific Adviser - Army (Doc Data Sheet and distribution list only)
Air Force Scientific Adviser
Director Trials

Aeronautical and Maritime Research Laboratory
Director
Chief of Weapons Systems Division
Mr M.C. Chick
Dr D. Whelan
Author(s): G. Bocksteiner

Mr N Ayres, WSD-S
Dr J.P. (John) Best, MOD-M
Dr N. Burman, SSMD-M
Dr J.M. Brett, SSMD-M
Mr M.C. Chick, WSD-M
Mr M. Chung, WSD-M
Mr J. Hooper, WSD-S (copies)
Mr B. Hamshere, WSD-S
Dr D. Jones, WSD-M
Mr A. Krelle, SSMD-M
Mr F.G. May, MOD-M
Mr D.Reitzel, WSD-M
MR R. Parker, WSD-M
Mr W. Reid, SSMD-M
Dr D.J. Whelan, WSD-M
Mr P. Whitty, ADI-M
Mr G. Yiannakopoulos, SSMD

DSTO Library
Library Fishermens Bend
Library Maribyrnong
Library DSTOS (2 copies)
Library, MOD, Pyrmont (Doc Data sheet)

c. Forces Executive

Director General Force Development (Sea)
Director General Force Development (Land), (Doc Data Sheet)
Director General Force Development (Air), (Doc Data Sheet)

d. Navy
SO (Science), Director of Naval Warfare, Maritime Headquarters Annex, Garden Island, NSW 2000. (Doc Data Sheet)

e. Army
ABCA Office, G-1-34, Russell Offices, Canberra (4 copies)

f. Air Force
No compulsory distribution

g. S&I Program
Defence Intelligence Organisation
Library, Defence Signals Directorate (Doc Data Sheet only)

h. Acquisition and Logistics Program
No compulsory distribution

i. B&M Program (libraries)
OIC TRS, Defence Central Library
Officer in Charge, Document Exchange Centre (DEC), 1 copy
DEC requires the following copies of public release reports to meet exchange agreements under their management:
*US Defence Technical Information Centre, 2 copies
*UK Defence Research Information Centre, 2 copies
*Canada Defence Scientific Information Service, 1 copy
*NZ Defence Information Centre, 1 copy
National Library of Australia, 1 copy

2. UNIVERSITIES AND COLLEGES

Australian Defence Force Academy
Library
Head of Aerospace and Mechanical Engineering
Deakin University, Serials Section (M list)), Deakin University Library, Geelong, 3217
Senior Librarian, Hargrave Library, Monash University
Librarian, Flinders University

3. OTHER ORGANISATIONS

NASA (Canberra)
AGPS

OUTSIDE AUSTRALIA

4. ABSTRACTING AND INFORMATION ORGANISATIONS
INSPEC: Acquisitions Section Institution of Electrical Engineers
Library, Chemical Abstracts Reference Service
Engineering Societies Library, US
American Society for Metals
Documents Librarian, The Center for Research Libraries, US

5. **INFORMATION EXCHANGE AGREEMENT PARTNERS**

Acquisitions Unit, Science Reference and Information Service, UK
Library - Exchange Desk, National Institute of Standards and Technology, US

Additional Distribution

Naval Surface Warfare Center (Indian Head Division), White Oak Laboratories,
10901 New Hampshire Ave, Silver Spring, Maryland 20903-5000 USA
Attention: Dr M.M. Swisdak (1 copy)
Dr Jerry Forbes (1 copy)
Dr Erwin Anderson (1 copy)
Ahn Duong (1copy)
Leonard Lipton (1 copy)
Library (1 copy)

Australian Ordnance Council, Department of Defence, Campell Park Offices, Canberra ACT
Attention: Capt J. Murphy(1 copy)
Mr J. Kedge (Desk Officer) (1 copy)
Mr A. Hasib Khan (Contact Officer)(1 copy)

Manager Armament Engineering Support (MAES), Naval Support Command, Sydney
Attention: LCMDR C. Bartlett (1 copy)
RSNES Sydney (Attn LCMDR S. Day)
RSNES Melbourne (Attn Mr L.C. Sabin)
UK
Barry Richardson (DRA, Ft Halstead, Kent, UK),
Capt Peter Phillips RAN, Ordnance Board, UK
NIMIC, NATO HEADQUARTERS 1110 Brussels Belgium

Total number of copies: 70

DEFENCE SCIENCE AND TECHNOLOGY ORGANISATION
DOCUMENT CONTROL DATA

1. PRIVACY MARKING/CAVEAT (OF DOCUMENT)

2. TITLE

Evaluation of Underwater Explosive Performance of PBXW-115 (AUST)

3. SECURITY CLASSIFICATION (FOR UNCLASSIFIED REPORTS THAT ARE LIMITED RELEASE USE (L) NEXT TO DOCUMENT CLASSIFICATION)

Document	(U)
Title	(U)
Abstract	(U)

4. AUTHOR(S)

G. Bocksteiner

5. CORPORATE AUTHOR

Aeronautical and Maritime Research Laboratory
PO Box 4331
Melbourne Vic 3001

6a. DSTO NUMBER	6b. AR NUMBER	6c. TYPE OF REPORT	7. DOCUMENT DATE
DSTO-TR-0297	AR-009-488	Technical Report	February 1996

8. FILE NUMBER	9. TASK NUMBER	10. TASK SPONSOR	11. NO. OF PAGES	12. NO. OF REFERENCES
510/207/0198	Task Number	DARMENG (Navy)	35	29

13. DOWNGRADING/DELIMITING INSTRUCTIONS

To be reviewed three years after date of publication

14. RELEASE AUTHORITY

Chief, Weapons Systems Division

15. SECONDARY RELEASE STATEMENT OF THIS DOCUMENT

Approved for Public Release

OVERSEAS ENQUIRIES OUTSIDE STATED LIMITATIONS SHOULD BE REFERRED THROUGH DOCUMENT EXCHANGE CENTRE, DIS NETWORK OFFICE, DEPT OF DEFENCE, CAMPBELL PARK OFFICES, CANBERRA ACT 2600

16. DELIBERATE ANNOUNCEMENT

No Limitations

17. CASUAL ANNOUNCEMENT Yes

18. DEFTEST DESCRIPTORS

Underwater explosions
Plastic bonded explosives
Underwater ordnance
Performance tests

19. ABSTRACT

An investigation has been carried out on the underwater explosive performance properties of Australian-made PBXW-115, a polymer bonded explosive (PBX) made from AP / bimodal RDX / Al in a plasticised polyurethane binder. The following underwater performance parameters of 25 kg PBX-115 charges, detonated by a central core of pentolite, have been measured: peak pressure, time constant, shock impulse, energy flux density, shock wave energy, relative bubble energy and the similitude constants have been evaluated. The shock wave energy (E_{SW}) of PBXW-115 (Aust) is 1.85 and its bubble energy (E_{RB}) is 2.25, relative to the accepted standard, pentolite (values 1.00), for each parameter); these values compare to those from Composition H-6 (E_{SW} 1.18, E_{RB} 1.54) probably the most commonly used and best known underwater explosive amongst the current inventories of the navies of the world. These data suggest that PBXW-115 should be a superior fill for use in underwater blast weapons.